

# A Computational Fluid Model for Investigation of Plasma Waves and Instabilities

H. Hakimi Pajouh<sup>1\*</sup>, M. R. Rouhani<sup>2</sup>, H. Abbasi<sup>1,3</sup>, F. Kazeminejad<sup>4</sup>, and S. Rouhani<sup>5</sup>

<sup>1</sup>*Institute for Studies in Theoretical Physics and Mathematics, P. O. Box 19395-5531, Tehran, Iran*

<sup>2</sup>*Department of Physics, Az-zahra University, P. O. Box 19834, Tehran, Iran*

<sup>3</sup>*Faculty of Physics, Amir Kabir University of Technology, P. O. Box 15875-4413, Tehran, Iran*

<sup>4</sup>*Independent consultant*

<sup>5</sup>*Faculty of Physics, Sharif University of Technology, P. O. Box 11365-9161, Tehran, Iran*

A computational fluid model is developed to study waves and instabilities. A new technique involving initial perturbations in configuration space have been implemented to excite the plasma waves; i.e. the perturbations acting similar to a random velocity distribution in particle in cell (PIC) codes. This forms a new powerful tool for investigation of many waves arising in both thermal and cold plasmas and as such will allow investigation of problems demanding scales and resolution not yet possible by PIC codes. The model predicts Langmuir waves, two stream instabilities, nonlinear wave-wave interaction, and the Debye screening effects. The agreement between theory and simulation where analytic results are available are excellent.

## I. INTRODUCTION

Due to the fundamental importance of the waves and instabilities in plasma and hydrodynamics investigations, computational researchers have devoted great efforts in developing appropriate tools. One of the main challenges after developing numerically stable algorithms in fluid models has been generation of the waves in the linear, nonlinear as well as unstable modes; i.e. waves which preserve analytic dispersion relations<sup>1</sup> [2]. Furthermore extending the case of hydrodynamics to that of MHD and or plasma physics one deals with waves with considerably more complicated propagation characteristics than the hydrodynamics cases treated by those authors; i.e. dispersion, polarization, oblique propagations, etc.

The main problems in generating a wave spectrum from small amplitude disturbances in fluid equations are: (1) the highly nonlinear nature of those equations; (2) the lack of an initial thermal velocity distribution. The first problem could cause any small amplitude configuration space disturbance to grow to very large amplitudes in relatively short times and result in wave breaking and non-propagation. Also when there does exist a thermal distribution, there are always a distribution of thermalized particles in phase with most waves; they can therefore excite the allowed modes to at least half their thermal level. Therefore in a case without thermal equilibrium, a disturbance of arbitrary wavelength cannot strictly speaking apportion its energy to other allowed modes. For example in purely electrostatic cases, we know from equilibrium statistical mechanics that when there exist a thermal distribution each mode  $E_l(k)$  can acquire an energy [3]:

$$\frac{\langle |E_l(k)|^2 \rangle}{8\pi} \propto kT. \quad (1)$$

---

\*hakimi@theory.ipm.ac.ir

<sup>1</sup>The waves' propagation characteristics are encoded in the dispersion relations [1]

To investigate MHD wave spectra therefore magnetohydrodynamic particle codes have served as powerful tools [4], [6], [7], and [8]. For other plasma waves PIC [9] and [10] or hybrid codes [8], [11], and [12] have served as the main wave investigation tools; i.e., basically codes which start from thermal equilibrium. In these codes the random particle distribution acts like a disturbance in velocity space and configuration space remains unaltered at the beginning of each simulation.

In our case we initiate each simulation by a perturbation in configuration space. Despite the initial shape of the perturbation, we observe other allowed modes to develop similar to PIC simulations. We believe that the mesh discretization and the finite differencing contribute in the following ways: (i) round of errors alter the initial perturbation shape and can drive other wavelength; (ii) as the nonlinear effects grow amplitudes and shorten wavelengths to the numerical dissipation and dispersion scale lengths, these effects can act to dampen and initiate the propagation of the different modes and prevent indefinite nonlinear growth. These effects can therefore explain the observed wave spectra. With this then we can use fluid instead of PIC codes as a convenient alternative to investigate many waves.

The organization of the paper is as follows: in section II the model is treated analytically; in section III the numerical scheme (algorithm, stability and conservation laws) are presented; in section IV the various tests of the model are presented (test of the dispersion relation, two stream instability, screening effect and nonlinear harmonic generation). At the end a brief summary and conclusion with future direction are presented.

## II. ANALYTICAL TREATMENT

We focus on the investigation of the high frequency (hf) longitudinal waves; i. e. a frequency domain where ions can be safely assumed to form an immobile background ( $n_0$  represents their uniform density). The appropriate equations are then Poisson's and the electron fluid equations:

$$\frac{\partial n}{\partial t} + \frac{\partial}{\partial x}(nv) = 0, \quad (2)$$

$$\frac{\partial v}{\partial t} + v \frac{\partial}{\partial x} v = \frac{e}{m} \frac{\partial}{\partial x} \varphi - \frac{1}{nm} \frac{\partial P}{\partial x}, \quad (3)$$

$$\frac{\partial^2 \varphi}{\partial x^2} = 4\pi e(n - n_0). \quad (4)$$

Here  $\varphi$  is the self-consistent electric potential, and  $n$ ,  $v$ ,  $P$  and  $m$  represent the electron density, velocity, pressure and rest mass respectively. Without any loss of generality this problem is treated in one dimension. These basic equations are supplemented by an "equation of state" according to the particular thermodynamic properties of the fluid of interest. Here, isothermal equation of state is used:

$$P = nT, \quad (5)$$

where  $T$  is the electron temperature and is assumed to be constant and Boltzmann's constant,  $k$ , is assumed to be unity.

The minimum requirement of any computational model lies in its ability to preserve conservation laws; for that fluid equations are cast in flux conservative form. Equation (3) in conservative form upon using Eq. (5) in Eq. (3) becomes:

$$\frac{\partial v}{\partial t} + \frac{\partial}{\partial x} \left( \frac{1}{2}v^2 - \frac{e}{m}\varphi + \frac{T}{m} \ln n \right) = 0. \quad (6)$$

Note that the logarithmic term is caused by the electron pressure. Therefore the three equations that form the basis of our model are:

$$\frac{\partial n}{\partial t} + \frac{\partial}{\partial x}(nv) = 0, \quad (7)$$

$$\frac{\partial v}{\partial t} + \frac{\partial}{\partial x} \left( \frac{1}{2}v^2 - \frac{e}{m}\varphi + \frac{T}{m} \ln n \right) = 0, \quad (8)$$

$$\frac{\partial^2 \varphi}{\partial x^2} = 4\pi e(n - n_0). \quad (9)$$

We will next derive a dispersion relation for wave propagation using Eqs. (7), (8), and (9). To do this, linearizing Eqs. (7), (8), and (9) about a spatially uniform equilibrium ( $n = n_0 + \delta n$ ,  $v = \delta v$  and  $\varphi = \delta \varphi$ ), we obtain the following set:

$$\frac{\partial \delta n}{\partial t} + n_0 \frac{\partial}{\partial x} \delta v = 0, \quad (10)$$

$$\frac{\partial \delta v}{\partial t} + \frac{\partial}{\partial x} \left( -\frac{e}{m} \delta \varphi + \frac{1}{n_0} \delta n \right) = 0, \quad (11)$$

$$\frac{\partial^2 \delta \varphi}{\partial x^2} = 4\pi e \delta n. \quad (12)$$

Assuming simple plane wave solutions, Eqs. (10), (11), and (12) reduce to the following set of equations:

$$-i\omega \delta n + ikn_0 \delta v = 0, \quad (13)$$

$$-i\omega \delta v + ik \left( -\frac{e}{m} \delta \varphi + \frac{1}{n_0} \delta n \right) = 0, \quad (14)$$

$$-k^2 \delta \varphi = 4\pi e \delta n. \quad (15)$$

Eqs. (13), (14), and (15) yield nontrivial solution if the following is obeyed:

$$\omega^2 = \omega_p^2 + k^2 v_T^2, \quad (16)$$

where

$$\omega_p^2 = \frac{4\pi e^2 n_0}{m} \text{ and } v_T^2 = \frac{T}{m} \quad (17)$$

are the electron plasma frequency and the thermal velocity, respectively.

Studies of Langmuir waves (hf electron waves) are of particular importance. Aside from the applications to real experimental situations which will become evident in the application section, they serve as excellent probes for testing the validity of the fluid code that we have developed.

### III. NUMERICAL ALGORITHM

Our model is simply an intuitive construct based on well-known fluid dynamics and Poisson's equations, geared toward plasma physics applications, where many different wave phenomena in dispersive media are of interest. Its physical "conceptual basis" can be regarded as a model that treats non-stationary electron wave motion for hf domain where  $\omega \gg kv_T$  in linear and nonlinear regions. Besides, it can predict electron wave spectrum more accurately than "particle in cell simulation" as here we expect less numerical noise.

#### A. Normalization

In these calculations we use the following normalizations:

$$\omega_p t \rightarrow t, \quad \frac{x}{r_D} \rightarrow x, \quad \frac{v}{v_T} \rightarrow v, \quad \frac{n}{n_0} \rightarrow n, \quad \frac{e\varphi}{T} \rightarrow \varphi, \quad (18)$$

where

$$r_D^2 = \frac{T}{4\pi e^2 n_0} \quad (19)$$

is the electron Debye length. Using these definitions, Eqs. (2), (4), (6), and (16) can now be rewritten as follows:

$$\frac{\partial n}{\partial t} + \frac{\partial}{\partial x}(nv) = 0, \quad (20)$$

$$\frac{\partial v}{\partial t} + \frac{\partial}{\partial x} \left( \frac{1}{2}v^2 - \varphi + \ln n \right) = 0, \quad (21)$$

$$\frac{\partial^2 \varphi}{\partial x^2} = n - 1, \quad (22)$$

$$\omega^2 = 1 + k^2. \quad (23)$$

It is already mentioned, logarithmic term in Eq. (21) is caused by the electron pressure.. Thus the code has the flexibility of being easily converted to the case when electron pressure is negligible.

#### B. The Numerical Scheme

Next we shall describe the numerical scheme. The steps of the scheme are summarized in Table I. A Lax-Wendroff method is used to push  $n$  and  $v$ , while a poisson solver at the end of each step updates the electric potential.

The grid spacing and time step are denoted by  $\Delta$  and  $\Delta t$  respectively. The fluid velocity and density are known at integer time step  $l$ . To complete the initial conditions,  $\varphi$  is computed at the same time step ( $l$ ) by the help of a Poisson solver that is based on tridiagonal matrix method. Then  $n$  and  $v$  are pushed from  $l$  to  $l + 1/2$  as the auxiliary step of the Lax-Wendroff scheme using Eqs. (20) and (21) (please refer to item 3 of the Table I). Then again  $\varphi$  is computed in the auxiliary step ( $l + 1/2$ ) using the value of  $n$  in the mentioned step. Having known  $n$ ,  $v$ , and  $\varphi$  at the time step  $l + 1/2$ , we push  $n$  and  $v$  all the way to time step  $l + 1$  as the main step of the Lax-Wendroff scheme in Eqs. (20) and (21) (items 5 and 6 in Table I). The electric potential  $\varphi$  is then computed at the time step  $l + 1$  using  $n^{l+1}$ .

TABLE I	
Numerical Algorithm of the Fluid Model for Plasma Waves	
Initially we have: $n_m^l, v_m^l$	
1. Compute electric potential, $\varphi_m^l$ , using Poisson solver.	
2. Compute fluxes in continuity and momentum equation in main step:	
$(f_n)_m^l = n_m^l v_m^l,$	
$(f_v)_m^l = \frac{1}{2}(v_m^l)^2 - \varphi_m^l + \ln n_m^l.$	
3. Push velocity and density half a time step:	
$n_{m+1/2}^{l+1/2} = \frac{1}{2}(n_{m+1}^l + n_m^l) - \frac{\Delta t}{2\Delta} [(f_n)_{m+1}^l - (f_n)_m^l],$	
$v_{m+1/2}^{l+1/2} = \frac{1}{2}(v_{m+1}^l + v_m^l) - \frac{\Delta t}{2\Delta} [(f_v)_{m+1}^l - (f_v)_m^l].$	
4. Compute electric potential in half step, $\varphi_{m+1/2}^{l+1/2}$ , using $n_{m+1/2}^{l+1/2}$ .	
5. Compute fluxes in continuity and momentum equations in half step:	
$(f_n)_{m+1/2}^{l+1/2} = n_{m+1/2}^{l+1/2} v_{m+1/2}^{l+1/2},$	
$(f_v)_{m+1/2}^{l+1/2} = \frac{1}{2}(v_{m+1/2}^{l+1/2})^2 - \varphi_{m+1/2}^{l+1/2} + \ln n_{m+1/2}^{l+1/2}.$	
6. Push the velocity and density another half a time step:	
$n_m^{l+1} = n_m^l - \frac{\Delta t}{\Delta} [(f_n)_{m+1/2}^{l+1/2} - (f_n)_{m-1/2}^{l+1/2}],$	
$v_m^{l+1} = v_m^l - \frac{\Delta t}{\Delta} [(f_v)_{m+1/2}^{l+1/2} - (f_v)_{m-1/2}^{l+1/2}].$	
7. Compute electric potential in the main step, $\varphi_m^{l+1}$ , using $n_m^{l+1}$ .	

### C. Conservation Laws

Equations (19), (20) are in conservative form, and we demand that the corresponding difference equations to be equally conservative. More specifically, we expect finite difference scheme to conserve the mass density ( $\int_{-\infty}^{+\infty} n dx$ ), momentum and the energy of the system, irrespective of the errors incurred by the finite difference lattice.

To investigate the conservation laws, in what follows, a method compatible with both the auxiliary and the main steps will be presented [14]. That is, Eqs. (20) and (21) are integrated over each space-time cell ( $m$ ) of area  $\Delta t \Delta_m$  ( $\Delta t = t^{l+1} - t^l$ ) as follows:

$$\int_{t^l}^{t^{l+1}} dt \int_{\Delta_m} dx \frac{\partial n}{\partial t} = - \int_{t^l}^{t^{l+1}} dt \int_{\Delta_m} dx \frac{\partial}{\partial x} (nv), \quad (24)$$

$$\int_{t^l}^{t^{l+1}} dt \int_{\Delta_m} dx \frac{\partial v}{\partial t} = - \int_{t^l}^{t^{l+1}} dt \int_{\Delta_m} dx \frac{\partial}{\partial x} \left( \frac{1}{2} v^2 - \varphi + \ln n \right). \quad (25)$$

Here  $\int_{\Delta_m}$  denotes integral over the cell labelled by  $m$ . Carrying out trivial integration over  $dt$  and  $dx$  on the left and right sides respectively Eqs. (24) and (25) become:

$$\int_{\Delta_m} n^{l+1} dx - \int_{\Delta_m} n^l dx = - \int_{t^l}^{t^{l+1}} dt \sum_{\alpha} (nv)_m, \quad (26)$$

$$\int_{\Delta_m} v^{l+1} dx - \int_{\Delta_m} v^l dx = - \int_{t^l}^{t^{l+1}} dt \sum_{\alpha} \left( \frac{1}{2} v^2 - \varphi + \ln n \right)_m, \quad (27)$$

where  $\alpha$  stands for the boundaries of every cell (the right and the left). Using

$$\int_{\Delta_m} \begin{pmatrix} n^l \\ v^l \end{pmatrix} dx = \Delta \begin{pmatrix} n_m^l \\ v_m^l \end{pmatrix}. \quad (28)$$

the following equations are thus obtained:

$$n_m^{l+1} = n_m^l - \int_{t^l}^{t^{l+1}} dt \frac{1}{\Delta} \sum_{\alpha} (nv)_m \quad (29)$$

$$v_m^{l+1} = v_m^l - \int_{t^l}^{t^{l+1}} dt \frac{1}{\Delta} \sum_{\alpha} \left( \frac{1}{2} v^2 - \varphi + \ln n \right)_m. \quad (30)$$

Summing over cells ( $m$ ) in the system results in:

$$\sum_{m=1}^M (n_m^{l+1} - n_m^l) = - \sum_{m=1}^M \int_{t^l}^{t^{l+1}} dt \frac{1}{\Delta} \sum_{\alpha} (nv)_m, \quad (31)$$

$$\sum_{m=1}^M (v_m^{l+1} - v_m^l) = \sum_{m=1}^M \int_{t^l}^{t^{l+1}} dt \frac{1}{\Delta} \sum_{\alpha} \left( \frac{1}{2} v^2 - \varphi + \ln n \right)_m. \quad (32)$$

Since finite differences were used in computing all the derivatives, then if one sums over all the grid cells in the system, each such quantities will appear twice with opposite signs corresponding to the cell boundaries that are being shared between the neighboring cells, and they will thus add up to zero. There can, however, be contributions from the walls of the computation box. For the periodic boundary condition the walls contributions gives zero; for other cases appropriate boundary conditions are implemented to insure good conservation using guard cells.

#### D. Numerical Stability Analysis

In order to obtain the Courant-Fredricks-Lewy (CFL) condition for the model, the difference equations (obtained from the differential equations for the problem by discretizing them) must be considered. We follow the method of Potter [14]; *i.e.* obtain the integration time pusher operator from the difference equations assuming a spatially uniform system and solve them in Fourier space and obtain a non-local result. We shall do the stability analysis with the pressure term.

Recall that the differential equations (20), (21) and (22) formed the basis of the model. These equations upon linearization, give:

$$\frac{\partial \delta n}{\partial t} + \frac{\partial}{\partial x} \delta v = 0, \quad (33)$$

$$\frac{\partial \delta v}{\partial t} + \frac{\partial}{\partial x} (-\delta \varphi + \delta n) = 0, \quad (34)$$

$$\frac{\partial^2 \delta \varphi}{\partial x^2} = \delta n. \quad (35)$$

Next using Eqs. (33), (34), and (35), after combining the auxiliary and the main steps of the Lax-Wendroff scheme and assuming  $n$ ,  $v$ , and  $\varphi$  to have the form ( $l$  refers to the time step and  $m$  inside the parenthesis to the grid location along  $x$ )

$$(n^l, v^l, \varphi^l) = (\hat{n}^l, \hat{v}^l, \hat{\varphi}^l) e^{i(km\Delta)}, \quad (36)$$

we obtain the following integration matrix ( $\sigma = k\Delta/2$ ):

$$\begin{pmatrix} n \\ v \\ \varphi \end{pmatrix}^{l+1} = \begin{pmatrix} 1 - \frac{2\Delta t^2}{\Delta^2} \sin^2 \sigma & \frac{-2i\Delta t}{\Delta} \sin \sigma \cos \sigma & \frac{2\Delta t^2}{\Delta^2} \sin^2 \sigma \\ \frac{-2i\Delta t}{\Delta} \sin \sigma \cos \sigma - \frac{i\Delta\Delta t}{2} \cot \sigma & 1 - \frac{\Delta t^2}{2} - \frac{2\Delta t^2}{\Delta^2} \sin^2 \sigma & 0 \\ \frac{\Delta t^2}{2} - \frac{\Delta^2}{4\sin^2 \sigma} & \frac{i\Delta\Delta t}{2} \cot \sigma & -\frac{\Delta t^2}{2} \end{pmatrix} \begin{pmatrix} n \\ v \\ \varphi \end{pmatrix}^l \quad (37)$$

Thus, according to Von Neumann stability condition the following inequality should be held:<sup>2</sup>

$$|g_\mu| \leq 1, \quad (38)$$

where  $g_\mu$  are the eigenvalues of the integration matrix and subscript refer to different eigenvalues (here  $\mu = 1, 2, 3$ ).

The value of  $g_\mu$  is then determined by setting the following determinant equal to zero; i.e.,

$$\begin{vmatrix} 1 - \frac{2\Delta t^2}{\Delta^2} \sin^2 \sigma - g & \frac{-2i\Delta t}{\Delta} \sin \sigma \cos \sigma & \frac{2\Delta t^2}{\Delta^2} \sin^2 \sigma \\ \frac{-2i\Delta t}{\Delta} \sin \sigma \cos \sigma - \frac{i\Delta\Delta t}{2} \cot \sigma & 1 - \frac{\Delta t^2}{2} - \frac{2\Delta t^2}{\Delta^2} \sin^2 \sigma - g & 0 \\ \frac{\Delta t^2}{2} - \frac{\Delta^2}{4\sin^2 \sigma} & \frac{i\Delta\Delta t}{2} \cot \sigma & -\frac{\Delta t^2}{2} - g \end{vmatrix} = 0 \quad (39)$$

The corresponding solutions for  $g$  are simply:

$$g_1 = 0,$$

$$g_{2,3} = 1 - \frac{1}{2}\Delta t^2 - \frac{2\Delta t^2}{\Delta^2} \sin^2 \sigma \pm i\sqrt{\Delta t^2 \cos^2 \sigma \left(1 + \frac{4}{\Delta^2} \sin^2 \sigma\right)}. \quad (40)$$

$g_1$  fulfills the inequality (38). For the two other eigenvalues, we have:

$$|g_2| = |g_3| = \left[ 1 - \Delta t^2 \left(1 + \frac{4}{\Delta^2} \sin^2 \sigma\right) + \Delta t^4 \left(\frac{1}{4} + \cos^4 \sigma\right) \left(1 + \frac{4}{\Delta^2} \sin^2 \sigma\right)^2 \right]^{1/2} \quad (41)$$

Equation (38) is then obeyed if the following inequality is held:

$$\Delta t^2 \left(\frac{1}{4} + \cos^4 \sigma\right) \left(1 + \frac{4}{\Delta^2} \sin^2 \sigma\right) \leq 1. \quad (42)$$

Since  $\Delta t$  and  $\Delta$  are small values ( $0 < \Delta t \ll 1$  and  $0 < \Delta \ll 1$ ) the inequality (42) will be satisfied if:

$$\frac{\Delta t}{\Delta} \leq \frac{2}{\sqrt{4 + \Delta^2}}. \quad (43)$$

Inequality (43) is exact up to the scheme accuracy, however, taking into account the smallness of  $\Delta t$  and  $\Delta$  the following stability condition results:

$$\frac{\Delta t}{\Delta} \leq 1.$$

---

<sup>2</sup> $()^{l+1} = g()^l$  where  $g = e^{-i\omega\Delta t}$ ; Von Neumann stability condition holds for  $\omega$  real.

#### IV. TESTING THE CODE

As mentioned, we have constructed the one-dimensional version of the code and have tested it by looking at small and large amplitude (nonlinear) effects in an initially uniform plasma. In what follows, a review of the results will be given.

##### A. Dispersion relation

The most basic requirement of a computational model aside from conservation laws is its ability to predict the linear theory; e.g. the waves dispersion relation. The degree to which the analytic dispersion relation is obeyed acts as a gauge of the computational model and serves to determine its limitations.

From Eq. 40, the dispersion relation of the corresponding difference equation is:

$$e^{-\omega_I \Delta t} \sin(\omega_R \Delta t) = \sqrt{(\Delta t)^2 \cos^2 \sigma \left(1 + \frac{4}{\Delta^2} \sin^2 \sigma\right)}.$$

where  $\omega = \omega_R + \omega_I$ . Comparison of this with the analytic dispersion relation shows that by changing  $k \rightarrow k \sin(k\Delta)/(k\Delta)$  in the analytic case one roughly recovers the above result for  $\Delta t \omega_R \ll 1$ ,  $k\Delta \ll 1$ . The fact that  $\omega_I$  does not have any  $k$  dependence, implies no part of the  $k$  space to be more susceptible to numerical instability than others<sup>3</sup>. The difference dispersion relation above also indicates that for  $\sin(k\Delta)/(k\Delta) \rightarrow 1$  the numerical dispersion to disappear; i.e. for modes with wavelengths long compared with the grid spacing it should be negligible.

For the initial perturbations, small fluctuations in the density from a uniform background were implemented. Table 2. shows three different initial perturbations used in the simulations; i.e. :

$n(x) = 1 + 0.01 \sin(k_0 x)$
$n(x) = 1 + 0.01(-x + x^3)e^{-x^2}$
$n(x) = 1 + 0.01 \begin{cases} -1 + x & -1 \leq x < 0 \\ 1 - x & 0 \leq x \leq 1 \\ 0 & \text{Else where} \end{cases}$

The reason for these choices is that the first perturbation maintain harmonics with wave numbers very close to  $k_0$  while the latter two maintain harmonics more uniformly distributed in the  $k$  space. The most important reason for such choices was to determine the impact of the initial perturbations on the final wave spectra; strictly speaking the latter two are expected to give rise to more uniform spectra. The initial velocity profiles corresponding to these three profiles are drawn in Figs. 1(a), (b) and (c). These velocity profiles indicate broader and more uniform distribution of bulk flow velocities in the latter two; i.e. the volume of phase space available to wave propagations are considerably larger.

---

<sup>3</sup>Many PIC algorithms show  $\omega_I \propto k^2$ ; i.e. intense short wavelength noise or instability.



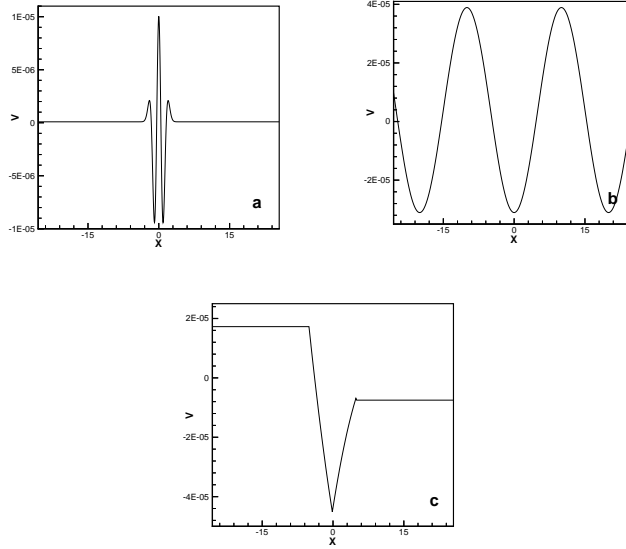


FIG. 1. Velocity profile for a)  $n(x) = 1 + 0.01(-x + x^3)e^{-x^2}$ , b)  $n(x) = 1 + 0.01 \sin(k_0 x)$  and c) Saw-tooth function

Given these two facts though, the plots of the power spectra<sup>4</sup> of the modes versus  $\omega$  (their frequency) indicate very close agreement in all the cases; i.e. regardless of the initially excited modes and phase velocities, most the allowed  $k$ -space tends to get excited. This supports our earlier claim that the discretization procedure and the numerical dispersion and dissipation have in effect broadened and stabilized the initial spectrum.

Finally the plots of the dispersion relation for a system size of  $1024\Delta$  with  $\Delta = 0.01$  are shown in Fig 2 and 3. The close agreement between the analytic theory (solid lines) and the model (circles) for wave numbers  $k$  as large as 6 indicate resolution of the modes with wave lengths of the order of grid spacing with negligible numerical dispersion. Comparison of these with the corresponding PIC simulations for a system  $256\Delta$  length (Fig. 4) clearly indicate resolution of much shorter wavelengths here and considerably less numerical dispersion. This is understandable since in the PIC models the finite particle size effects introduce additional numerical dispersion which cause smaller allowed  $k$ 's.

---

<sup>4</sup>The power spectrum is determined in two steps: First, the spatial FFT is used in a quantity (e.g.  $E(x,t)$ ) and stored  $E(k_i,t)$ , next for each  $k_i$  temporal FFT is performed on  $E(k_i,t)$

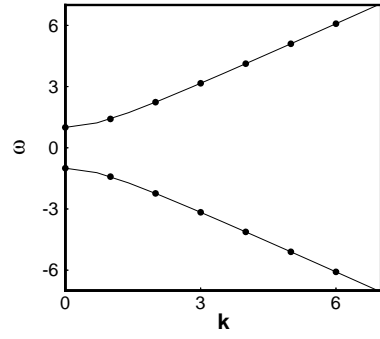


FIG. 2. Dispersion relation for Langmuir wave.

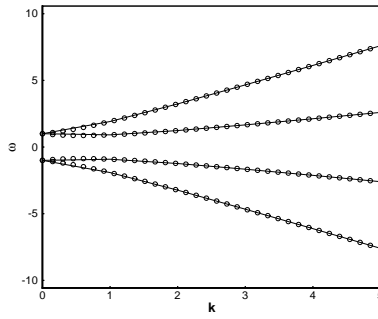


FIG. 3. Dispersion relation for Langmuir wave with Doppler effect

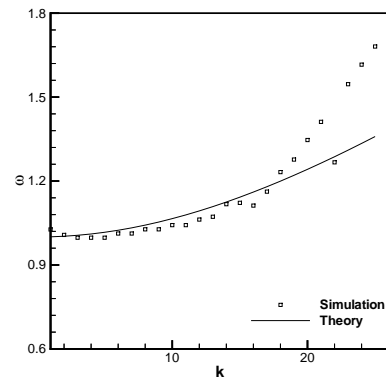


FIG. 4. Dispersion relation for Langmuir wave for a typical PIC simulation

One last remark about the cases corresponding to Figs. 2 and 3 is that the latter involves the case in which the bulk plasma had an initial flow velocity. Fig. 3 not only shows that the doppler shifted waves also obey their respected dispersion relation, it also shows how any "resulting" plasma flow could impact those waves. That is if any nonzero average flow should arise from the initial perturbations (i.e. if the scheme does not preserve momentum conservation ) the dispersion relation would be impacted as in Fig. 3. A glance at Fig. 2 though points that there could not have been any doppler shift and therefore no net plasma flow must have resulted from the initial perturbations. Calculations also showed that  $\langle v_f \rangle = 0$  initially remained so to round off errors throughout the simulation. So these plots also probe the momentum to be conserved in the model.

### B. Wave Launching on the Boundary

In the next example a wave is launched from the boundary and its behavior is followed. Theoretically, recall that in an unmagnetized plasma and in the linear regime the plasma shields any incoming AC density perturbation whose frequency is less than plasma frequency ( $\omega_p$ ). This effect is shown in Fig. 5(b) and Fig. 6. In this example the frequency of the applied density perturbation is half of the plasma frequency. The wave is launched at  $x = -25\lambda_D$ . The amplitude of the density perturbation has the following range: nonlinear (0.2,1.8) Fig. 5(a) and linear (0.99,1.01) Fig. 5(b)<sup>5</sup>. The penetration depth is from  $x = (-25, -20)$  in the linear and  $x = (-25, -15)$  in the nonlinear case. Furthermore as Fig. 6(a) indicates, upon penetration, after one wave period following the first crest ( $x = -18$ ), the second crest steepens with its wavelength decreasing to grid cell scale.<sup>6</sup> In the linear regime though [Fig. 6(b)] no steepening can be seen.

---

<sup>5</sup>In these particular shots the wave trough fall at launch points.

<sup>6</sup>The oscillations are numerical in nature. The model should be modified to include FCT filter [15] to eliminate these spurious oscillations.

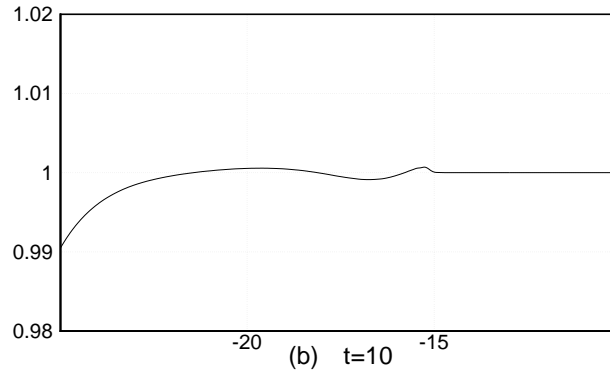
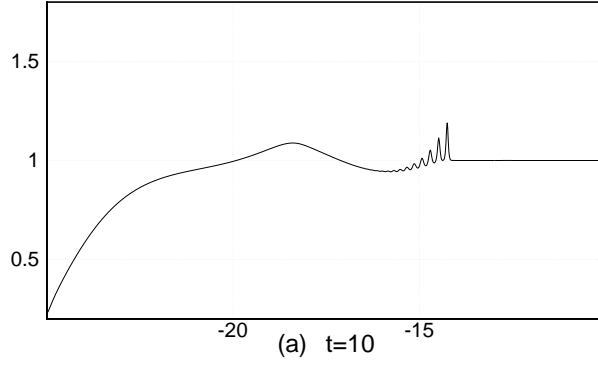


FIG. 5. Non-linear and linear penetration of electric field (both plots are sketched at  $t=10$ ). a) Nonlinear case b) linear case

In the other case, with the same initial condition (respect to linear case), we launched a wave whose frequency was larger than the plasma frequency ( $\omega > \omega_p$ ). This time the density perturbation propagated into the plasma with its wavelength and amplitude unchanged as it penetrated the plasma. Its behavior also conformed with the analytic dispersion relation. The results are shown in Fig. 7.

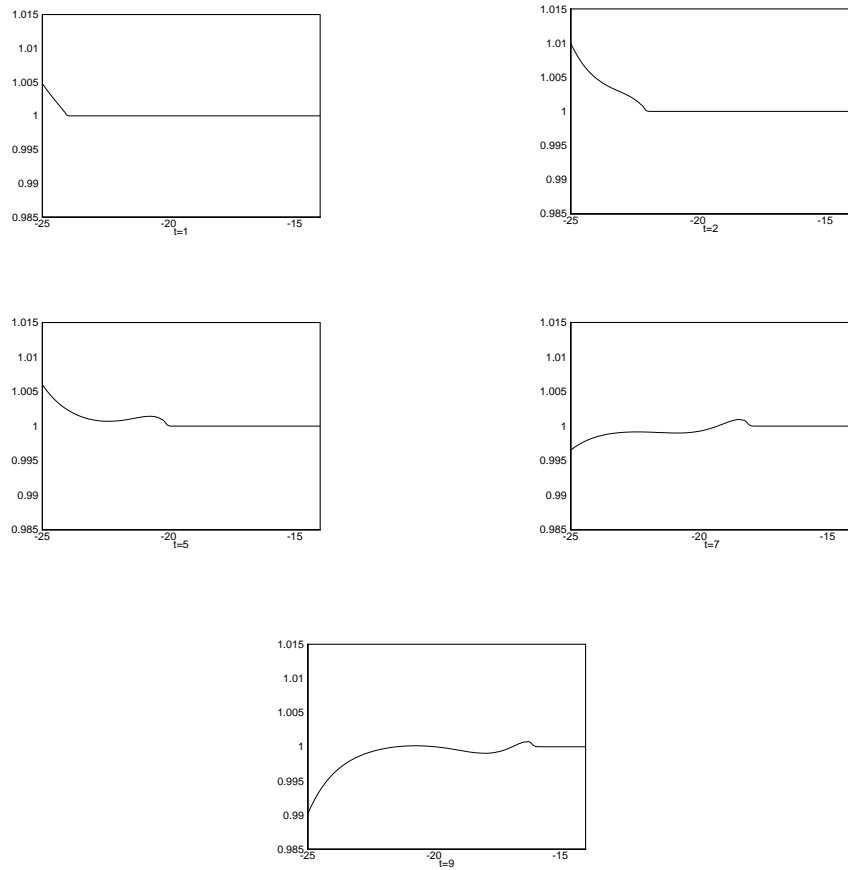


FIG. 6. Density versus the position when the external frequency is half of the plasma frequency. To give a time evolution feeling, they are plotted for five different normalized time.

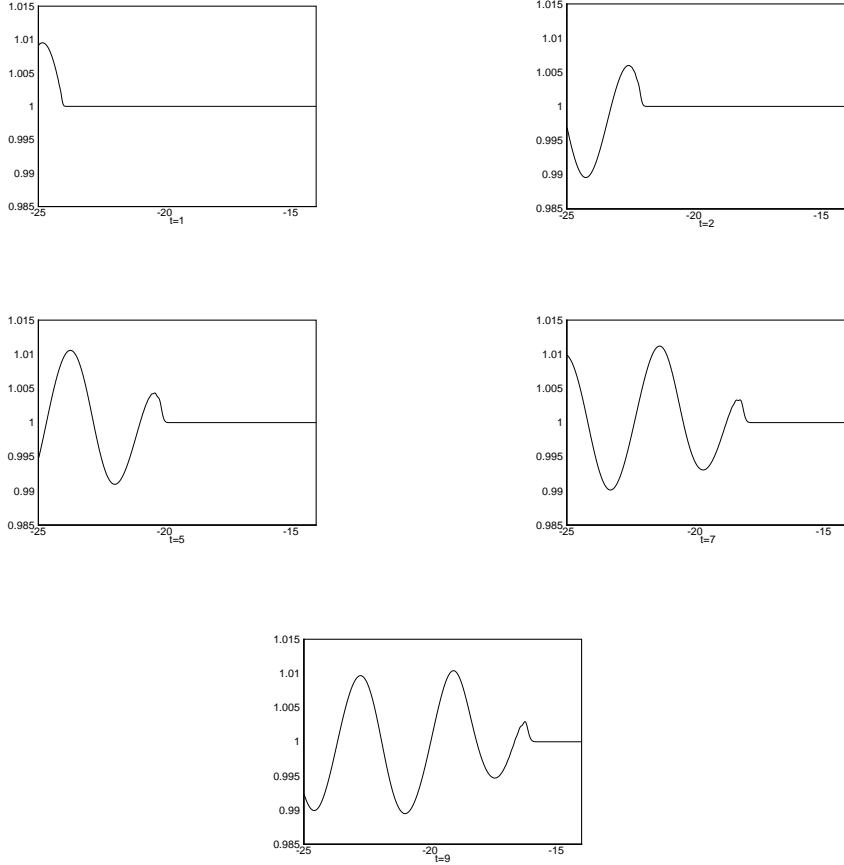


FIG. 7. Density versus the position when the external frequency is two times of the plasma frequency. To give a time evolution feeling, they are plotted for five different normalized time.

### C. Two Stream Instability

As a more severe test of the code, we treated the two stream instability. Although the instability arises under a wide range of beam conditions, we shall consider only the simple case of two counterstreaming uniform beams of electrons with the same number density  $n_0$ . The first beam travels in the x direction with drift velocity  $v_d$  and the second beam in the opposite direction with same drift velocity, i.e. the counterstreaming beams have the same speed. The dispersion relation is as follows:

$$\frac{\omega_p^2}{(kv_d - \omega)^2} + \frac{\omega_p^2}{(kv_d + \omega)^2} = 1 \quad (44)$$

where  $\omega_p^2 = 4\pi e^2 n_0 / m$  is the same plasma frequency for both beams. One can then obtain the following expression for  $\omega^2$ :

$$\omega^2 = \omega_p^2 + k^2 v_d^2 \pm \omega_p (\omega_p^2 + 4k^2 v_d^2)^{1/2}. \quad (45)$$

This relationship between  $\omega^2$  and  $k^2$  is shown graphically in Fig. 8. It is clear that, there exists a critical wave number  $k_c$  which separates the stable and unstable modes. In fact, for  $k^2 < k_c^2$  two values of  $\omega$  are complex, one of which

represents a growing wave; i.e. an instability. Moreover, there exists a wave number  $k_m$  that corresponds to the most unstable mode.

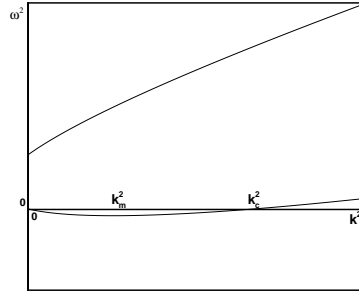


FIG. 8. Representation of relationship between  $\omega^2$  and  $k^2$ .

These effects are examined by the fluid code. In this case the code was generalized to a two counterstreaming fluid model. As the two counterstreaming beams emerging from the opposite ends meet half way into the simulation box, a growing wavelike disturbance develops. Figs. 9 and 10 show the evolution of this disturbance for the cases with and without the pressure terms respectively. In both cases the disturbance grows locally while in the latter it also begins to propagate in both directions; i.e. a result of the dispersion due to the pressure term.

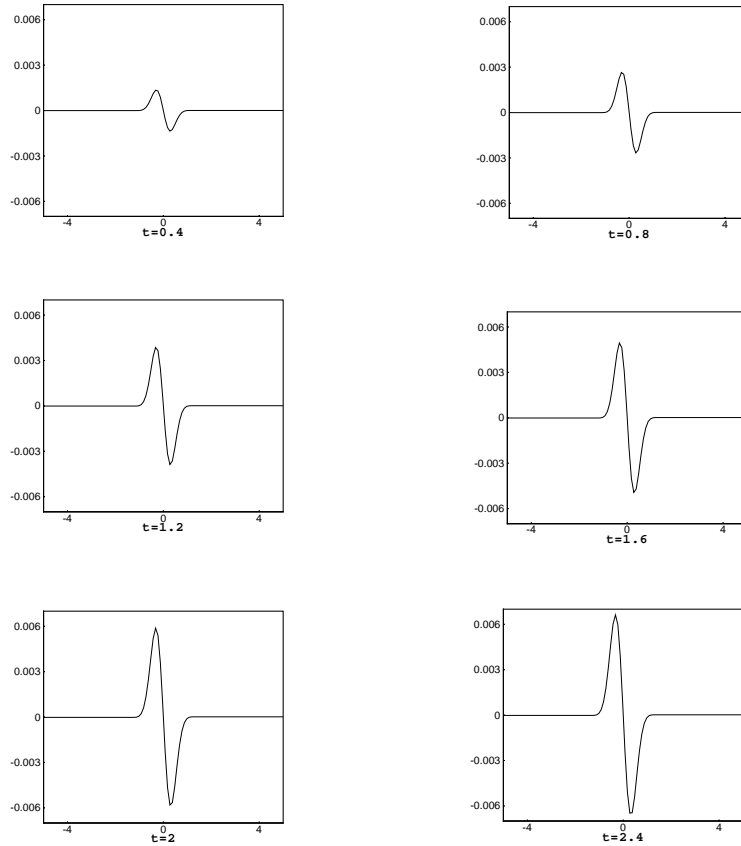


FIG. 9. Electric field versus the position in absence of pressure. Time is normalized by  $\omega_p$ .

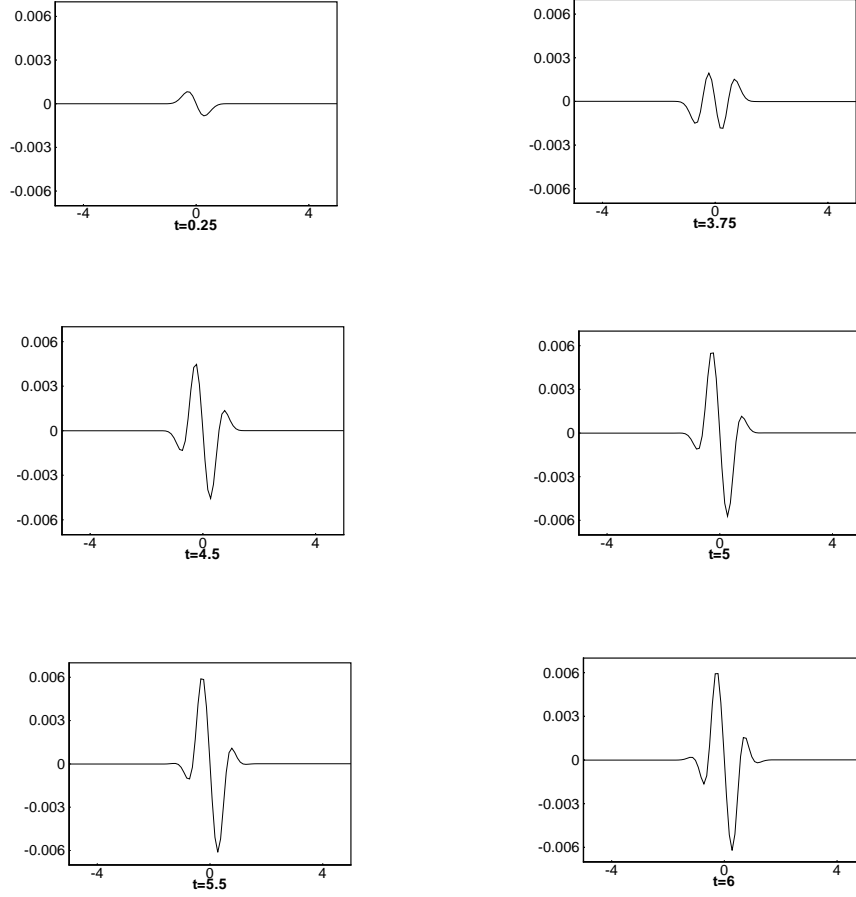


FIG. 10. Electric field versus the position in presence of pressure. Time is normalized by  $\omega_p$ .

Furthermore, the instability of each mode was investigated using the mode energy discussed in the previous section: i.e.

$$P(k, t) = |E(k, t)|^2 \quad (46)$$

The time derivative of this function with respect to  $k$  is shown in Fig. 11. As expected, there exists a critical wave number below which unstable modes can grow. Furthermore we observed the the most unstable mode corresponding to  $k = k_m$  as the maximum in the Fig. 11. Also the dynamic evolution of the beam-beam interaction was observed as a movie and both the disturbance growth and upstream propagations (when pressure term was included) were observed.



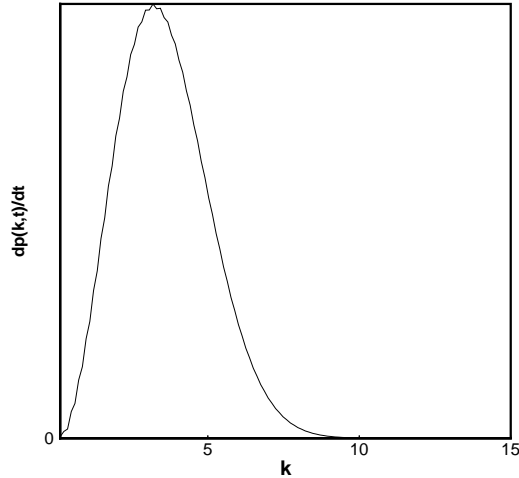


FIG. 11.  $dp(k,t)/dt$  versus  $k$ . Cutoff and maximum wave numbers ( $k_c, k_m$ ) are comparable with theory.

## V. CONCLUSION

The result of this paper demonstrates that fluid model can be used to investigate any waves predicted by their basic set of equation. This can include waves of kinetic nature with and without dispersion with resolution far greater than the corresponding PIC codes. It was demonstrated that appropriate initial perturbations coupled with difference algorithms of sufficient but not excessive numerical dispersion and dissipation can give rise to wave spectra spanning all the allowed k-space. Many areas of plasma and or space research can greatly benefit from these techniques.

- [1] Whitham G. B., *Linear and nonlinear waves*, Wiley, NewYork, 1974.
- [2] Tam C. K. and Webb J. C., *J. Comput. Phys.*,107, 262-281,1993.
- [3] Dawson J. M., *Rev. Mod. Phys.* Vol 2,241,1983.
- [4] Leboeuf J. N., Tajima T., and Dawson J. M., *J. Comput. Phys.* **38**, 237 (1980).
- [5] J. Von Neumann and R. D. Richtmyer, *J. Appl. Phys.* **21**, 232 (1950).
- [6] Tajima T., Leboeuf J. N., and Dawson J. M.,*J. Comp. Phys.*, **38**, 237,1980.
- [7] Brunel F., Leboeuf J. N., Tajima T., and Dawson J. M., it *J. Comp. Phys.*, **43**, 268,1981.
- [8] Kazeminezhad F., Leboeuf J. N., Brunel F., and Dawson J. M., *J. Comp. Phys.*, Vol 104, 2, 1993.
- [9] Birdsall C. K., and Langdon A. b., *Plasma physics via computer simulation*, (Mc Graw-Hill, New York), 1995.

- [10] Hockney R. W. and Eastwood J. W., *Computer simulation using particle*, (IOP publishing Ltd.), 1988.
- [11] Winske D., *Space Sci. Rev.*, **42**, 53, 1985.
- [12] Horowitz E. J., Schumaker D. E., and Anderson D. V., *J. Comp. Phys.*, **84**, 279, 1989.
- [13] Kazeminezhad F., Leboeuf J. N., Sydora R., and Holland D., *J. Comp. Phys.*, **102**, 277, 1992.
- [14] Potter D. E., *Computational Physics* (Wiley, New York, 1973), Chap. 3.
- [15] Boris J. P. and Book D. L., *J. Comp. Phys.***11**, 38 1973.